# Dalton Transactions

## PAPER

Check for updates

# Nanocomposites based on hierarchical porous carbon fiber@vanadium nitride nanoparticles as supercapacitor electrodes†

Fen Ran, [iD] *[a,b] Yage Wu,[a] Minghuan Jiang,[a] Yongtao Tan,[a] Ying Liu,[a] Lingbin Kong, [iD] [a,b] Long Kang[a,b] and Shaowei Chen [iD] *[c]

In this study, a hybrid electrode material for supercapacitors based on hierarchical porous carbon fiber@vanadium nitride nanoparticles is fabricated using the method of phase-separation mediated by the PAA-$b$-PAN-$b$-PAA tri-block copolymer. In the phase-separation procedure, the ionic block copolymer self-assembled on the surface of carbon nanofibers, and is used to adsorb $NH_4VO_3$. Thermal treatment at controlled temperatures under an $NH_3 : N_2$ atmosphere led to the formation of vanadium nitride nanoparticles that are distributed uniformly on the nanofiber surface. By changing the PAN to PAA-$b$-PAN-$b$-PAA ratio in the casting solution, a maximum specific capacitance of 240.5 F g$^{-1}$ is achieved at the current density of 0.5 A g$^{-1}$ with good rate capability at a capacitance retention of 72.1% at 5.0 A g$^{-1}$ in an aqueous electrolyte of 6 mol L$^{-1}$ KOH within the potential range of −1.10 to 0 V (rN/A = 1.5/1.0). Moreover, an asymmetric supercapacitor is assembled by using the hierarchical porous carbon fiber@vanadium nitride as the negative electrode and Ni(OH)$_2$ as the positive electrode. Remarkably, at the power density of 400 W kg$^{-1}$, the supercapacitor device delivers a better energy density of 39.3 W h kg$^{-1}$. It also shows excellent electrochemical stability, and thus might be used as a promising energy-storage device.

## 1. Introduction

Energy storage technologies are vital for efficient utilization of energy. Among the energy storage devices, supercapacitors show practical applications and have been attracting much attention, owing to their high power density, good cycling stability, fast charging–discharging capability, and safe operation.[1–6] Much progress has been made to overcome the major barriers of low energy density without sacrificing the power density or cycle life.[7–14] According to $E = 0.5CV^2$ ($E$ is the energy density, $C$ is the capacitance, and $V$ is the operating voltage window), enhancing $C$ and widening $V$ can be employed to increase the energy density of super-capacitors.[15,16] The original polymer-based and bio-based carbon materials (unmodified by functional groups such as

nitrogen- and oxygen-containing) usually suffer from lower level specific capacitances, where the capacitance comes from the charge separation at an electrode/electrolyte interface.[3,17–21] Hence, a number of studies have been focused on metal oxides and conducting polymers because of their high pseudocapacitance through fast reversible redox reactions.[22–25] But they are usually used as positive electrode materials. Transition metal nitrides have been widely investigated for supercapacitors, such as VN,[26–30] WN,[31] TiN,[32,33] Mo$_x$N,[34,35] and so on, as important negative electrode materials, owing to their superb electrical conductivity (4000–55 500 S cm$^{-1}$), high capacitance (>200 F g$^{-1}$), and wide operating potential window (0.8–3 V). Among them, vanadium nitride (VN) has attracted considerable attention. In fact, a variety of VN nanostructures have been constructed as super-capacitive negative electrodes, such as nanoparticles, nano-fibers, and nanotubes.[15,36–38]

The performance may be enhanced by the deposition of VN nanostructures on a porous carbon substrate. Polyacrylnitrile (PAN) is a typical hydrocarbon for the synthesis of carbon-aceous materials,[39–41] where the –CN functional group may enable *in situ* nitrogen doping during the carbonization process.[42] Electrospinning is a useful method to shape PAN into high-surface-area one-dimensional (1D) nanofibers.[43,44] With *in situ* N doping, PAN nanofibers have been used as a

[a]State Key Laboratory of Advanced Processing and Recycling of Non-ferrous Metals, Lanzhou University of Technology, Lanzhou 730050, P. R. China.
E-mail: ranfen@163.com
[b]School of Material Science and Engineering, Lanzhou University of Technology, Lanzhou 730050, Gansu, P. R. China.
[c]Department of Chemistry and Biochemistry, University of California, 1156 High Street, Santa Cruz, California 95064, USA. E-mail: shaowei@ucsc.edu
†Electronic supplementary information (ESI) available. See DOI: 10.1039/c7dt04432a

substrate for loading active catalytic nanoparticles, including Ag, Au, and Pd.[45] Until now, the main synthetic method for preparing VN/carbon composite materials has been the chemical deposition of transition-metal oxides or nitrides onto porous carbon materials.[46–48] However, the loading of vanadium is limited by the subsurface area and compatibility of the base. Therefore, it is necessary to develop effective loading methods, which can not only lead to an accurate loading of the vanadium-based groups but also prevent aggregation of the VN nanoparticles.

Herein, we report a facile strategy for the preparation of hierarchical porous carbon fiber@vanadium nitride nanoparticles (HPCF@VNNP) by pyrolysis of triblock copolymer blended polymer nanofibers loaded with vanadium precursors. In comparison with the previous preparation of VN/C-based electrode materials, this method offers several distinct benefits: (i) through the self-assembly of ionic and amphiphilic block copolymers on the nanofiber surface, the active materials can be loaded uniformly on the carbon surface, which helps enhance the usage efficiency of the active material; (ii) by varying the amount of the block copolymer, the content of the active materials can be accurately controlled; and (iii) high carbon content with considerable N-doping in the composite material enhances the electronic conductivity and contact wettability. Consequently, based on the advanced structure architecture, the fabricated HPCF@VNNP exhibits good electrochemical performance, such as good specific capacitance and energy density, and long stability.

## 2. Experimental

### 2.1 Chemicals

Vinylcyanide (AN) and acrylic acid (AA) from Sinopharm Chemical Reagents Co. Ltd were purified by distillation prior to use. Azobisisobutryonitrile (AIBN) was purchased from Tianjin Tianhe Chemical Reagent Factory (Tianjin, China) and used as received. Ammonium metavanadate ($NH_4VO_3$, analytical reagent), ethyl ether, and $N,N$-dimethylformamide (DMF) were purchased from Sinopharm Chemical Reagents Co. Ltd, and used as received without any further purification. A RAFT agent was synthesized according to the literature.[49]

### 2.2 Preparation of the polyacrylonitrile (PAN) precursor

PAN was synthesized by solution polymerization according to the previous work.[50,51] Typically, AN (19.2 g), and AIBN (0.056 g) were dissolved in 60 mL of DMF under magnetic stirring at 70 °C for 6 h. After the reaction, the sample was precipitated with ethanol. And the resulting precipitate was washed thoroughly with distilled water several times. Finally the product was dried under vacuum at 40 °C for 24 h.

### 2.3 Synthesis of PAA-b-PAN-b-PAA

Synthesis of the macro-RAFT agent of –PAA: AA, RAFT agent, AIBN, and DMF were added into a tube. After bubbling for 30 min with nitrogen, the reaction mixture was allowed to warm under a nitrogen atmosphere to 75 °C, and the polymerization lasted for 4 h. After precipitation in ethyl ether, the product was dried under vacuum at 60 °C overnight.

Synthesis of the PAA-b-PAN-b-PAA triblock copolymer: AN, the macro-RAFT agent (–PAA), AIBN, and DMF were added to a tube, and stirred for 10 min. After bubbling with nitrogen for 30 min, the reaction mixture was allowed to warm to 75 °C under a nitrogen atmosphere and polymerization was carried out for 12 h. After precipitation in ethyl ether, the product was dried under vacuum at 60 °C overnight.

### 2.4 Preparation of triblock copolymer blended polymer nanofibers

Triblock copolymer blended polymer nanofibers were prepared by the electrospinning technique. Typically, PAN (1.5 g) and PAA-b-PAN-b-PAA (0.1–1.5 g) were added into DMF, which was heated at 60 °C for 3 h to obtain a homogeneous solution. The electrospinning solution was put into a 20 mL plastic syringe connected to a transparent flexible polyethylene pipe closely with a stainless steel needle, which was fixed perpendicular to the water surface. A positive potential of 23.0–24.0 kV was applied between the needle tip and water surface at a distance of 10.0 cm. The flow rate of the electrospinning solution was 0.6 mL h$^{-1}$.

### 2.5 Adsorption of vanadium-based groups

A $NH_4VO_3$ solution was prepared at a concentration of 0.12 mol L$^{-1}$ in distilled water at 60 °C. Polymer nanofibers were then added into the solution, and soaked at 60 °C for 24 h under magnetic stirring. After that, the samples were dried at 60 °C under an air flow for 24 h and further used as precursors.

### 2.6 Preparation of hierarchical porous carbon fiber@vanadium nitride nanoparticles (HPCF@VNNP)

The precursors were pre-heated under an air flow at 270 °C for 1 h to achieve pre-oxidation, and then heated under a mixed atmosphere of $NH_3 : N_2 = 3 : 2$ at 800 °C for 1 h in a tubular furnace. The heating rate was controlled at 5 °C min$^{-1}$.

### 2.7 Structure characterization

The microstructure of the as-prepared materials was characterized by FTIR measurements with a Nicolet Nexus 670 FTIR instrument and a transmission electron microscope (TEM, JEOL JEM-2010). X-ray photoelectron spectroscopy (XPS) measurements were carried out with a Physical Electronics instrument, and X-ray diffraction (XRD) patterns were acquired with a Rigaku D/MAX 2400 diffractometer (Cu Kα radiation λ = 1.5418 Å, operated at 40 kV and 60 mA). Energy dispersive X-ray (EDX) spectroscopy, thermogravimetric analysis (TGA), and differential scanning calorimetry (DSC) were carried out to estimate the amount of each ingredient in the sample. The surface morphology of the samples was examined with a field emission scanning electron microscope (SEM, JEOL JSM-6700F).

## 2.8 Electrochemical measurements

A typical three-electrode system was used to evaluate the electrochemical performance of the sample. All electrochemical measurements were carried out using a CHI660 electrochemical analyzer with a platinum foil as the counter electrode. A saturated calomel (SCE) and Ni foam of 1 cm$^2$ in area were used as the reference electrode and the current collector, respectively. Typically, for a three-electrode system, the working electrode was prepared by coating the active material (80.0 wt%, 4.0 mg), acetylene black (7.5 wt%, 0.4 mg), polytetrafluoroethylene (5.0 wt%, 0.25 mg), and conducting graphite (7.5 wt%, 0.4 mg) onto a current-collector. After drying in a vacuum oven at 60 °C for 8 h, the nickel foam that was coated with active materials was pressed at a pressure of 10.0 MPa for 30 s in order to enhance the adhesion between the active materials and the current collector. The electrochemical tests including cyclic voltammetry (CV), galvanostatic charge discharge (GCD), and electrochemical impedance spectroscopy (EIS) were carried out using an electrochemical workstation. The CV curves were obtained at varying sweep rates from 5.0 to 50.0 mV s$^{-1}$, and GCD tests were conducted at various current densities from 0.5 to 5.0 A g$^{-1}$ in the potential window range of −1.1 to 0 V. For the EIS measurement, the frequency varied from 0.01–10$^5$ Hz and data were acquired at the open circuit voltage with the alternate current amplitude of 10.0 mV. The cycling test was performed using a LAND CT2001A instrument at a current density of 2.0 A g$^{-1}$.

Calculations: The specific capacitance of the electrode can be calculated from the discharging curves at different current densities by the equation:

$$C = It/(\Delta Vm) \quad C_m = It/m \tag{1}$$

where $C$ (F g$^{-1}$) is the specific capacitance and $C_m$ (C g$^{-1}$) is the specific charge, $I$ (A) is the discharge current, $t$ (s) is the discharge time, $\Delta V$ (V) is the potential drop during the discharge process and $m$ (g) is the mass of active materials.

The energy and power density of the device are calculated from the discharge curves at different current densities using the following equations:

$$E = CV^2/7.2 \tag{2}$$

$$P = 3600E/(\Delta t) \tag{3}$$

where $E$ (W h kg$^{-1}$) is the energy density of the device, $C$ (F g$^{-1}$) is the specific capacitance, $V$ (V) is the potential drop during the discharge process, $P$ (W kg$^{-1}$) is the power density of the device, and $\Delta t$ (s) is the discharge time.

## 3. Results and discussion

The detailed fabrication process of the hierarchical porous carbon fiber@vanadium nitride nanoparticles (HPCF@VNNP) is illustrated in Scheme 1. It includes four main steps: preparation of triblock copolymer blended polymer nanofibers, adsorption of vanadium-based groups, preoxidization and heat
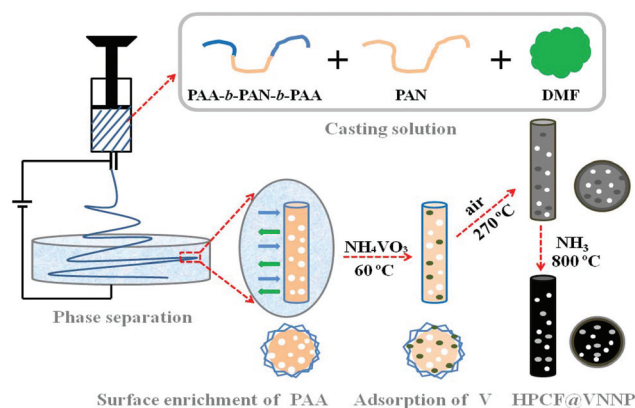


**Scheme 1** Schematic illustration of the synthesis process for HPCF@VNNP.

treatment. The detailed procedure is described in the Experimental section, starting with an ionic amphiphilic triblock copolymer of polyacrylic acid-*b*-polyacrylonitrile-*b*-polyacrylic (PAA-*b*-PAN-*b*-PAA), which was synthesized by reversible addition–fragmentation chain-transfer (RAFT) polymerization. Characterization data of PAA-*b*-PAN-*b*-PAA by FTIR and $^1$H NMR technologies are included in Fig. S1 in the ESI.† Casting solutions involving PAN, PAA-*b*-PAN-*b*-PAA, and solvents were prepared and transferred into a syringe, which were used to fabricate triblock copolymer blended polymer nanofibers by electrospinning technology. The nanofibers were obtained in a water bath, where the phase separation occurred. During the phase-separation, the solvent exchange and the migration of the block copolymer with solvent movement generated a hierarchical porous structure. Meanwhile, with fast solvent exchange of DMF and water, PAA-*b*-PAN-*b*-PAA migrated to the nanofiber surface, where –PAA blocks were exposed on the surface and –PAN blocks incorporated in the interior. The hydrophobic property of the –PAN block helped in minimizing the loss of PAA-*b*-PAN-*b*-PAA during the preparation procedure, while the ionic and hydrophilic property of the –PAA block was exploited for the loading of NH$_4$VO$_3$ on the nanofiber surface and in the hierarchical pores. After that, the materials were subject to a pre-heated process under an air flow at 270 °C for 1 h, and then in a mixed atmosphere of N$_2$ and NH$_3$ at 800 °C for 1 h, leading to the formation of HPCF@VNNP. The polymer nanofibers would remain and generate hierarchical porous carbon nanofibers, while NH$_4$VO$_3$ adsorbed on the fiber surface was transformed to VN nanoparticles.

Fig. 1 shows the SEM and TEM images of HPCF and HPCF@VNNP, both of which showed nanofibers with a uniform shape and a similar diameter in the range of 40 to 80 nm. SEM images of HPCF showed that HPCF had a smooth surface with a slightly curved shape that might result from the semicrystalline nature of the PAN precursor, as the swollen PAN domains partially crystallized and formed crosslinked structures during subsequent thermal stabilization[52] (Fig. 1a and b). In comparison, from Fig. 1c and d, one can see that the HPCF@VNNP sample maintained the fibrous morphology
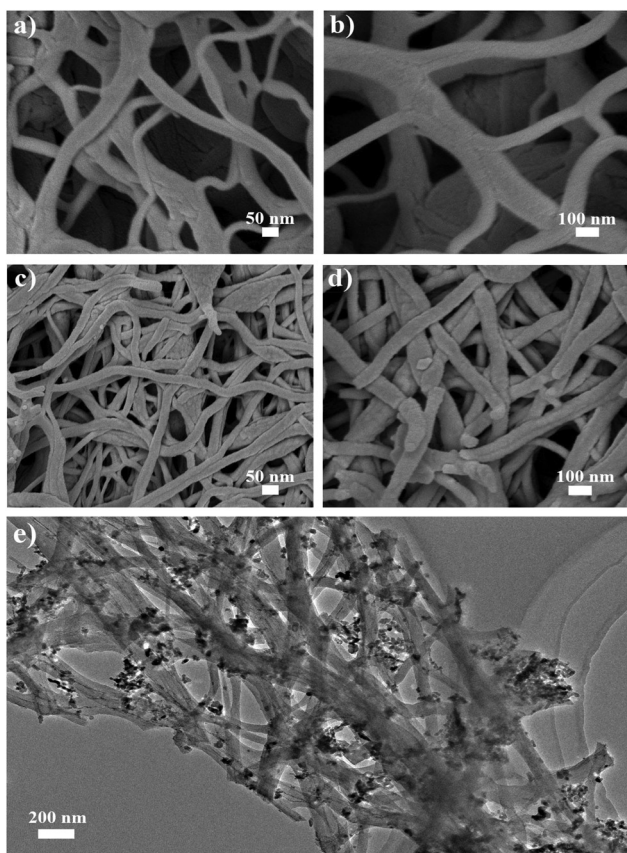
**Fig. 1** SEM images of (a, and b) HPCF, and (c, and d) HPCF@VNNP; and (e) TEM image of HPCF@VNNP.

diameter in the range of 70 to 90 nm with a somewhat rough surface caused by the loading of VN nanoparticles. Furthermore, from the TEM image of HPCF@VNNP, VN nanoparticles were obviously observed on the surface throughout all of the fibrous network (Fig. 1e). The VN nanoparticles were about 10 nm and showed no apparent aggregation due to the use of ionic block copolymers of PAA-*b*-PAN-*b*-PAA to carry the vanadium precursor before heat treatment.

As shown in Fig. 2, TEM, selected-area electron diffraction, EDS, and elemental mapping analyses were carried out to further study the microstructure of HPCF and HPCF@VNNP nanofibers. HPCF showed a diameter of 80 nm and revealed the presence of some mesopores and micropores with several nanometers in size, which might arise from solvent exchange during phase-separation and the electrospinning process (Fig. 2a and b, Fig. S2†). Furthermore, there were a number of VN nanoparticles scattered across the surface and inside the fibers (Fig. 2d). Because of the deposition of VN nanoparticles on the carbon surface, HPCF@VNNP showed a larger diameter of about 100 nm. SAED measurements showed very low crystallinity of HPCF, and good crystallinity of HPCF@VNNP, as manifested in Fig. 2h and i. EDX analysis for both HPCF and HPCF@VNNP, as shown in Fig. 2c and f, confirmed the inclusion of the V element in HPCF@VNNP. In addition, Fig. 2g shows the elemental mapping images of the

HPCF@VNNP hybrid material, where the elements of carbon, vanadium, nitrogen, and oxygen were homogeneously distributed throughout the entire nanofiber. The O signal was likely due to the surface oxidation of VN.[46] As such, the obtained HPCF@VNNP nanofibers showed the advanced structure of a higher crystallinity, uniform VN nanoparticles, and good porosity, which would be helpful to reduce the resistance of ions and electron transfer.

XPS, XRD, and BET measurements were then used to examine the composition of HPCF@VNNP, as shown in Fig. 3. The C 1s spectrum showed three fitting peaks: the peak at 284.8 eV can be ascribed to $sp^2$ hybridized carbon in C–N groups, and the other two peaks at 285.4 and 287.1 eV can be assigned to C–OH, and C=O bonds, respectively[53,54] (Fig. 3a). In the N 1s XPS spectrum of the HPCF@VNNP, two well-defined peaks were observed at 401.0, and 398.6 eV, corresponding to the graphitic (N–Q) produced in the nitrogen-doped carbon section and metal nitride [N (1s): 396.8–398.9 eV] of VN, respectively[55,56] (Fig. 3b). As shown in Fig. 3c, the characteristic peaks of O 1s, V $2p^{1/2}$, and V $2p^{3/2}$ were usually studied together because their binding energies were very close. The O 1s spectrum was divided into two main peaks at 531.1 and 532.7 eV, respectively. The peak at 531.1 eV demonstrated the existence of a complex mixture of vanadium oxides on the HPCF@VNNP surface, which included vanadium oxides with different valence states of V that were not transformed to nitrides completely under the thermal treatment conditions.[57] The other peak at 532.7 eV supported the existence of –OH groups on the HPCF@VNNP surface,[58] which can also improve the wettability of the electrode to the electrolyte and enlarge the contact area between the electrode and electrolyte, a characteristic that will further enhance the electrochemical performance of the material. The peaks centered at 514.1, and 521.6 eV belonged to the vanadium in VN,[58,59] while the peaks at 517.2, and 524.1 eV were ascribed to the V–O component on the material surface.[60] Therefore, based on the analysis of the XPS spectra, it could be confirmed that HPCF@VNNP is mainly composed of VN and carbon, together with a small amount of complex vanadium oxides on the surface. As shown in Fig. 3d, the XRD patterns of HPCF@VNNP displayed a broad peak at 22°, due to amorphous carbon derived from the PAN nanofiber precursor, which would contribute to the electrical conductivity of the product. Moreover, one relatively strong peak was observed at 43.8° due to the (200) crystal planes, and two weak peaks at 37.7° and 63.7° that may be indexed to the (111), and (220) diffractions of cubic VN (JCPDS Card no.73-0528), demonstrating that the vanadium-based groups were successfully converted into VN.[61]

Nitrogen adsorption–desorption measurements were then utilized to characterize the pore texture and pore size distribution of the prepared carbon materials, as shown in Fig. 3e and f. Apparently, the curve (Fig. 3e) showed a typical IV isotherm with an H3-type hysteresis loop at the pressure of $P/P_0 > 0.4$, confirming a loose network and coexisting micro-, meso-, and macropores in HPCF@VNNP.[62] The pore size distribution
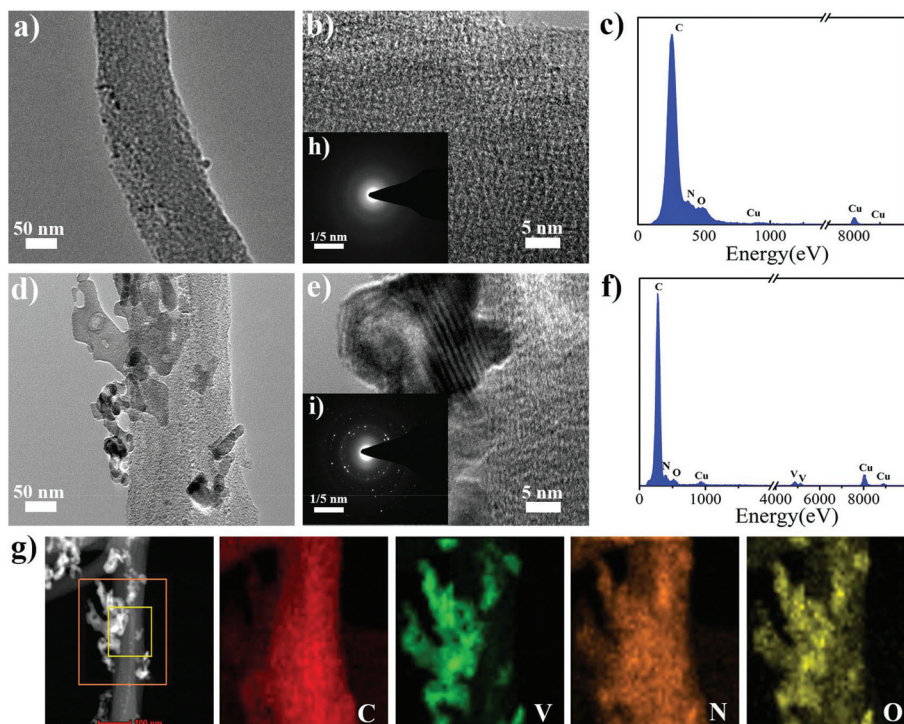
**Fig. 2** TEM images and the related energy dispersive X-ray spectra of a single nanofiber of (a–c) HPCF, and (d–f) HPCF@VNNP (inset is the selected-area electron diffraction pattern); and (g) elemental mapping images of C, V, N, and O elements.
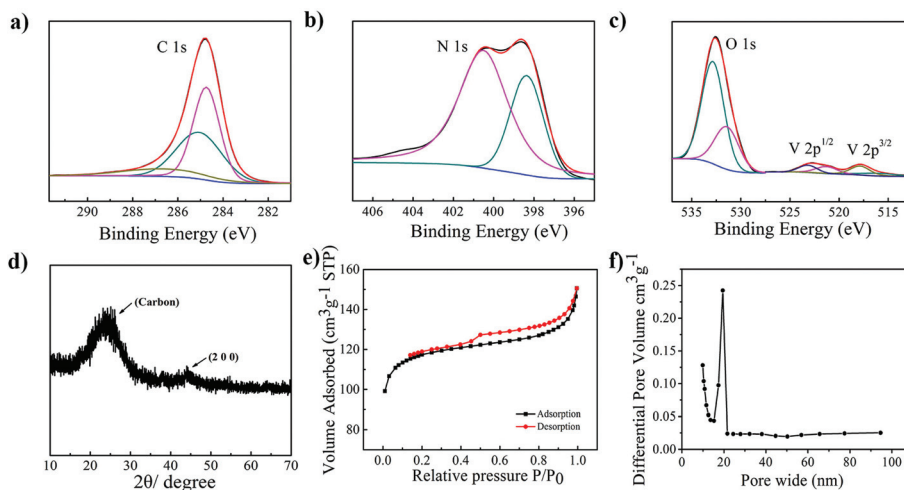


**Fig. 3** X-ray photoelectron spectra of (a) C 1s, (b) N 1s, and (c) O 1s and V 2p for HPCF@VNNP, (d) X-ray diffraction pattern, (e) N$_2$ adsorption–desorption isotherms, and (f) pore size distribution of HPCF@VNNP.

of HPCF@VNNP showed a range from 2.0 to 100.0 nm (Fig. 3f) with an average pore radius of 19.4 nm calculated by the BJH method using the adsorption branch of the isotherm. This abundant mesoporous structure was important for efficient diffusion and transport pathways to the interior voids of the materials, and thus may enhance the rate capability of the electrode.[63] It is worth mentioning that the BET surface area of the HPCF@VNNP was 357.8 m$^2$ g$^{-1}$, far higher than the values reported recently for various VN materials (Table S1†).

The high BET surface area is mainly due to the process of adsorbing –V that did not destroy the structure of PAN nanofibers, providing more active sites for the electrochemical process.

Homogeneous dispersion of VN nanoparticles on hierarchical porous carbon fibers and the rational design of the VN/carbon value predominantly depended on the feed ratio of PAN to PAA-*b*-PAN-*b*-PAA (rN/A) during the preparation of spinning solution. We thus systematically investigated the effect of
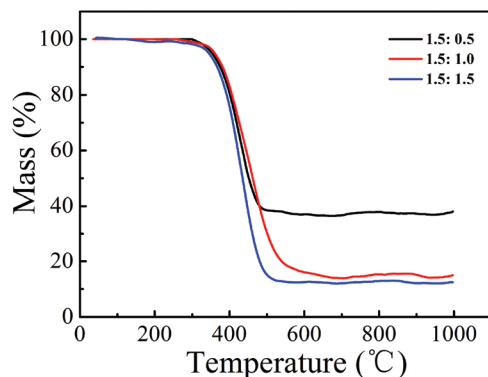
**Fig. 4** TGA curves of HPCF@VNNPs mediated by feeding various amounts of triblock copolymer.



**Fig. 5** The electrochemical capacitance performance of HPCF@VNNP mediated by various amounts of triblock copolymer: (a) CV, (b) GCD, (c) electrochemical impedance spectroscopy curve; and (d) specific capacitance at different current densities of 0.5, 1.0, 2.0, 3.0, 4.0, and 5.0 A $g^{-1}$, respectively.

rN/A, and the HPCF@VNNPs prepared at rN/A = 1.5 : 0.1 to 1.5 : 1.5 were named HPCF@VNNP-0.1 to HPCF@VNNP-1.5, respectively. The process of thermal decomposition and the constituent contents of the different HPCF@VNNP samples were further examined by simultaneous thermogravimetric analysis in air, as shown in Fig. 4. All samples were heated from room temperature to 1000 °C at a heating rate of 10 °C min$^{-1}$. With the increase of temperature, all curves firstly ascended and subsequently descended when the temperature was increased from 200 to 500 °C. These results were mainly due to the duplicate effect between the combustion weight loss of carbon and oxidation weight gain of VN. Furthermore, VN began to transform into V ~ N ~ O and further to $V_2O_5$ starting at 400 °C which caused the mass increase;[64] and at 500 °C, a dramatic loss took place owing to the transformation of carbon in the product into $CO_2$. The mass ratios of VN to carbon for HPCF@VNNP-0.5, HPCF@VNNP-1.0, and HPCF@VNNP-1.5 were calculated to be 27 : 73, 11 : 89, and 9 : 91, respectively.

The effect of rN/A on the electrochemical performance of HPCF@VNNPs was investigated by CV, GCD, and EIS measurements in a 6.0 M KOH aqueous solution with a three-electrode setup at room temperature, as shown in Fig. 5. All HPCF@VNNP samples showed a similar shape of the CV and charging/discharging curves (Fig. 5a and b). The CV curves of HPCF@VNNPs had a quasi-rectangular shape with two obvious symmetrical redox peaks, showing a typical characteristic of both double layer and redox processes. In addition, the redox peaks first became stronger and then weaker with a decreasing rN/A value. According to the calculation, the mass specific capacitances of HPCF@VNNP-0.1 to HPCF@VNNP-1.5 were 69.1, 127.5, 141.1, 204.6, 210.8, 176.2, and 136.5 F g$^{-1}$ at a current density of 1.0 A g$^{-1}$, respectively. EIS tests were then carried out over a frequency range of 0.01–10$^5$ Hz (Fig. 5c). The Nyquist plot featured a high phase-angle impedance plot and a low faradaic charge transfer resistance, indicating the fast ion transfer behavior of HPCF@VNNPs. Typically, HPCF@VNNP-1.0 exhibited a smaller equivalent series resistance and faster ion transfer due to the high BET surface area where the rich carbon content from nitrogen-doping not only
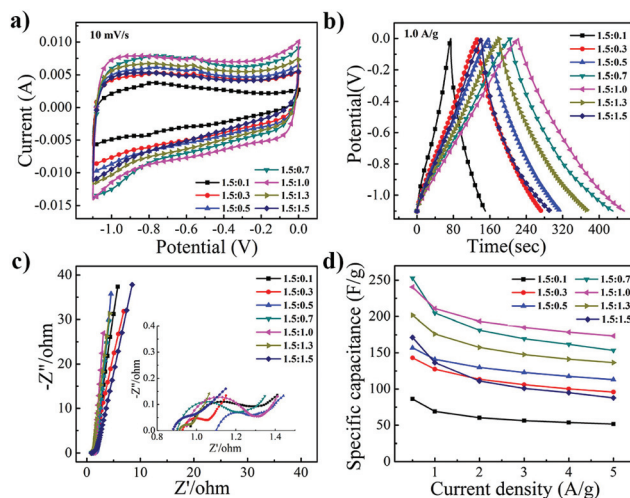
facilitated the diffusion and penetration of electrolyte ions to abundant pores but also improved the electrical conductivity.[65] Fig. 5d shows the specific capacitances at different current densities. As the current density increased from 0.5 to 5.0 A g$^{-1}$, the retention values of the capacitance for HPCF@VNNP-0.1 to HPCF@VNNP-1.5 were 59.8, 67.0, 71.9, 60.7, 72.1, 67.7 and 51.3%, respectively. One can see that HPCF@VNNP-1.0 exhibited the best overall electrochemical performance. These data confirmed that the rN/A value, that means the ratio of VN to carbon in the electrode material, played an important role in the electrochemical storage process: at too high or too low rN/A value, a high supercapacitor performance cannot be obtained.

The detailed electrochemical properties of HPCF@VNNP-1.0 are shown in Fig. 6. In all CV curves collected at different scan rates (from 5.0 to 50.0 mV s$^{-1}$), a pair of broad redox peaks were observed in the potential range from −1.1 to 0 V (Fig. 6a), indicating the capacitive mechanism of HPCF@VNNP composed of both electrical double layer capacitance and pseudo capacitance from faradaic reactions.[66] Interestingly, even at high scan rates, the shape of the voltammograms did not change drastically, manifesting superior capacitive behavior of the electrode materials. Fig. 6b shows the GCD curves for HPCF@VNNP-1.0 between −1.1 and 0 V at a current density of 0.5 to 5.0 A g$^{-1}$. The almost linear profiles and symmetrical triangle shape corroborated the dominating capacitive characteristic as well as outstanding reversibility and rate capability during the process of charge storage. Importantly, there was no apparent voltage drop (iR) related to the internal resistance during the change of polarity, which also manifested nearly perfect capacitive behavior.[67] These results were consistent with the CV data. The specific capacitances of the samples tested at a current density of 0.5, 1.0,
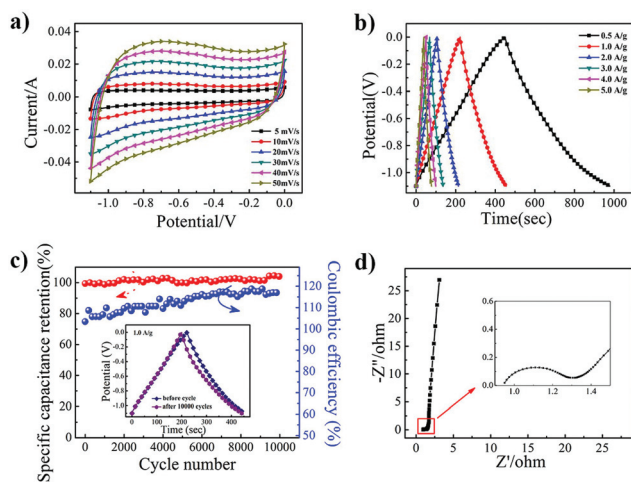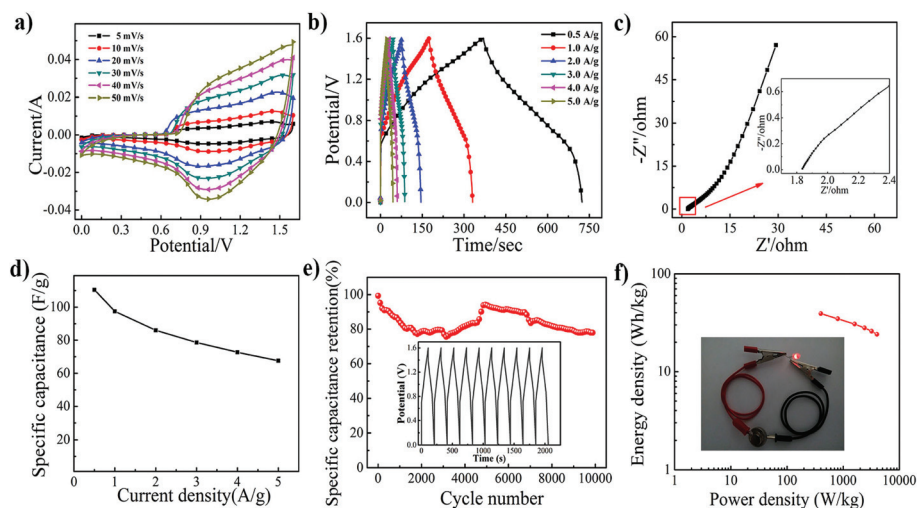
Fig. 6 The electrochemical capacitance performance of HPCF@VNNP-1.0: (a) CV curves at various scanning rates; (b) GCD curves at various current densities; (c) cycle life and columbic efficiency (inset is the GCD comparison after 10 000 cycles); and (d) electrochemical impedance spectra.

2.0, 3.0, 4.0, and 5.0 A g$^{-1}$ were estimated to be 240.5, 210.8, 193.5, 185.1, 178.5, and 173.4 F g$^{-1}$, respectively, higher than those reported earlier with other VN/C-based nanofibers.[4,27,29] Significantly, the sample had a good cycling stability in 6 M KOH aqueous solution (Fig. 6c) with a high capacitance retention of 98% even after 10 000 cycles at 2.0 A g$^{-1}$, and the coulombic efficiency retained 115%. The GCD curves recorded after 10 000 cycles showed that the sample still maintained the initial capacity, demonstrating the good electrochemical reversibility with promising potential in the application of energy storage devices.

To simulate the actual device behavior, the active material of HPCF@VNNP was used as the negative electrode and Ni(OH)$_2$ as the positive electrode to assemble a hybrid supercapacitor, HPCF@VNNP||Ni(OH)$_2$. The electrochemical performance of the pristine Ni(OH)$_2$ nanoparticles is also given in Fig. S3 in the ESI.† Moreover, to build a supercapacitor with high operating voltage and high energy density, charge storage on the positive and negative electrodes maintains the relationship of q+ = q−. To balance the charge storage, the mass matching of the positive and negative electrodes was optimized by using the equation: $m_+/m_- = (C_- \times \Delta V_-)/(C_+ \times \Delta V_+)$, where m is the mass of the electrode material, $C$ is the specific capacitance of the electrode material, and $\Delta V$ is the potential drop of the positive or negative electrode during the discharging process. In this study, the calculated optimal mass ratio of Ni(OH)$_2$ and HPCF@VNNP was 1 : 2.1. Hence, in a two-electrode system, the mass loading of Ni(OH)$_2$ and HPCF@VNNP was 1.9 mg and 4.0 mg respectively. Fig. 7a depicts the CV curves of HPCF@VNNP||Ni(OH)$_2$ in the voltage range from 0 to 1.6 V at scan rates of 5.0 to 50.0 mV s$^{-1}$. A couple of oxidation and reduction peaks were observed, indicating pseudocapacitive properties corresponding to the redox reactions on the surface of positive Ni(OH)$_2$ and negative HPCF@VNNP hybrids. The specific capacitances of the hybrid device HPCF@VNNP||Ni(OH)$_2$ at different current densities from 0.5 to 5.0 A g$^{-1}$ at 0–1.6 V were calculated from the GCD curves to be 110.4, 97.4, 86.0, 78.6, 72.7, and 67.6 F g$^{-1}$, respectively (Fig. 7b), confirming the high specific capacitance and good capacitive behavior of the ASC. As shown in Fig. 7c, the EIS of the hybrid devices was obtained at room temperature with the frequency range from 0.01–10$^5$ Hz. It had a small intercept at the real axis of 1.81 Ω, reflecting lower equivalent series resistance in the electrochemical system (inset in Fig. 7c). Moreover, the Nyquist plots featuring vertical curves in the low-frequency region indicated lower ion diffusive resistivity and nearly ideal capacitive behavior in devices. From the data, about 61.3% of specific capacitance was retained when the



Fig. 7 The electrochemical capacitance performance of the HPCF@VNNP||Ni(OH)$_2$ ASC device: (a) CV curves at various scanning rates; (b) GCD curves at various current densities; (c) electrochemical impedance spectroscopy curve; (d) specific capacitance at different current densities of 0.5, 1.0, 2.0, 3.0, 4.0, and 5.0 A g$^{-1}$, respectively; (e) cycle life (inset shows the cycle life and columbic efficiency); and (f) Ragone plot.

current density was changed from 0.5 to 5 A $g^{-1}$ for the hybrid device (Fig. 7d). Fig. 7e shows the electrochemical stability of HPCF@VNNP based hybrid supercapacitors HPCF@VNNP||Ni(OH)$_2$ tested at a current density of 2.0 A $g^{-1}$. Obviously, the hybrid device showed 78.2% retention of the original capacitance after 10 000 cycles. The superior cycling stability can be ascribed to the unique VN nanoparticles embedded in the hierarchical porous carbon fiber in which the carbon matrix not only enhanced the electrical conductivity but also accommodated the volume changes of VN and prevented their aggregation during cycling processes.[68]

Energy density and power density are two additional important parameters for the evaluation of the entire device, and the Ragone plot is shown in Fig. 7f. One can see that at a power density of 400 W $kg^{-1}$, the HPCF@VNNP||Ni(OH)$_2$ ASC delivered a high energy density of 39.3 W h $kg^{-1}$. Even when the power density was increased to 4000 W $kg^{-1}$, the energy density remained at 24.1 W h $kg^{-1}$. Table S2 in the ESI† compared the electrochemical performances of the various VN-based electrodes reported in the literature. Notably, the devices fabricatedusing HPCF@VNNP||Ni(OH)$_2$ materials showed far superior performances compared to the literature results. In fact, the inset in Fig. 7f shows that the assembled device in series can light up a red LED, proving that the device has good application performance.

## 4. Conclusions

In summary, hierarchical porous carbon fiber@vanadium nitride nanoparticles (HPCF@VNNP) were successfully prepared by phase-separation mediated with a tri-block copolymer and high temperature calcination in an atmosphere of $NH_3 : N_2 = 3 : 2$ for high performance supercapacitors. The structure was characterized by XRD, SEM, TEM, and BET measurements showing the formation of hierarchical pores in the carbon fiber and high distribution of vanadium nitride nanoparticles. The reduced aggregation of the VN nanoparticles improved the electrical conductivity and the stability of the electrode material. The prepared HPCF@VNNP showed good electrochemical behaviors in a 6 M KOH aqueous electrolyte, with a specific capacitance of 240.5 F $g^{-1}$ at a current density of 0.5 A $g^{-1}$ and a good rate capability with a capacitance retention of 72.1% at 5.0 A $g^{-1}$. Notably, the hybrid device consisting of Ni(OH)$_2$ as the positive electrode and HPCF@VNNP as the negative electrode exhibited an ultrahigh energy density of 39.3 W h $kg^{-1}$ at a power density of 400 W $kg^{-1}$, and the energy density remained at 24.1 W h $kg^{-1}$ even when the power density was increased to 4000 W $kg^{-1}$. These results indicated that HPCF@VNNP is a promising electrode material for high-performance supercapacitors.

## Conflicts of interest

There are no conflicts to declare.

## Acknowledgements

## References

1 F. Cheng, J. Liang, Z. Tao and J. Chen, Functional materials for rechargeable batteries, *Adv. Mater.*, 2011, **23**, 1695–1715.

2 M. Zhang, Y. Qiu, Y. Han, Y. Guo and F. Cheng, Three-dimensional tungsten nitride nanowires as high performance anode material for lithium ion batteries, *J. Power Sources*, 2016, **322**, 163–168.

3 X. Xia, D. Chao, Y. Zhang, J. Zhan and Y. Zhong, Generic synthesis of carbon nanotube branches on metal oxide arrays exhibiting stable high-rate and long-cycle sodium-ion storage, *Small*, 2016, **12**, 3048–3058.

4 M. Balogun, M. Yu, Y. Huang, C. Li and P. Fang, Binder-free Fe$_2$N nanoparticles on carbon textile with high power density as novel anode for high-performance flexible lithium ion batteries, *Nano Energy*, 2015, **11**, 348–355.

5 K. Wiesener, D. Ohms, G. Benczúr-Ürmössy, M. Berthold and F. Haschka, High power metal hydride bipolar battery, *J. Power Sources*, 1999, **84**, 248–258.

6 G. Wang, L. Zhang and J. Zhang, A review of electrode materials for electrochemical supercapacitors, *Chem. Soc. Rev.*, 2012, **41**, 797–828.

7 V. Augustyn, P. Simon and B. Dunn, Pseudocapacitive oxide materials for high-rate electrochemical energy storage, *Energy Environ. Sci.*, 2014, **7**, 1597–1614.

8 X. Xia, D. Chao, Y. Zhang, Z. Shen and H. Fan, Three-dimensional graphene and their integrated electrodes, *Nano Today*, 2014, **9**, 785–807.

9 M. Salanne, B. Rotenberg, K. Naoi and K. Kaneko, Efficient storage mechanisms for building better supercapacitors, *Nat. Energy*, 2016, **1**, 16070.

10 T. Lin, I. Chen, F. Liu, C. Yang, H. Bi and F. Xu, Nitrogen-doped mesoporous carbon of extraordinary capacitance for electrochemical energy storage, *Science*, 2015, **350**, 1508–1513.

11 Y. F. Zhao, S. F. Huang, M. R. Xia, S. Rehman, S. C. Mu, Z. K. Kou, Z. Zhang, Z. Y. Chen, F. M. Gao and Y. L. Hou, N-P-O co-doped high performance 3D graphene prepared through red phosphorous-assisted "cutting-thin" technique: A universal synthesis and multifunctional applications, *Nano Energy*, 2016, **28**, 346–355.

12 Y. F. Zhao, W. Ran, J. He, Y. Z. Huang, Z. F. Liu, W. Liu, Y. F. Tang, D. W. Gao and Y. L. Hou, High-Performance asymmetric supercapacitors based on multilayer MnO2/

graphene oxide nanoflakes and hierarchical porous carbon with enhanced cycling stability, *Small*, 2015, **11**, 1310–1319.

13 Y. F. Zhao, W. Ran, J. He, Y. F. Song, C. M. Zhang, D. B. Xiong, F. M. Gao, J. S. Wu and Y. Y. Xia, Oxygen-rich hierarchical porous carbon derived from artemia cyst shells with superior electrochemical performance, *ACS Appl. Mater. Interfaces*, 2015, **7**, 1132–1139.

14 Z. Zhang, S. C. Mu, B. W. Zhang, L. Tao, S. F. Huang, Y. Z. Huang, F. M. Gao and Y. F. Zhao, A novel synthesis of carbon nanotubes directly from an indecomposable solid carbon source for electrochemical applications, *J. Mater. Chem. A*, 2016, **4**, 2137–2146.

15 A. Burke, Ultracapacitors: why, how, and where is the technology, *J. Power Sources*, 2000, **91**, 37–50.

16 Y. Gogotsi and P. Simon, True performance metrics in electrochemical energy storage, *Science*, 2011, **334**, 917–918.

17 J. Liu, T. Yang, D. Wang, G. Q. M. Lu, D. Zhao and S. Z. Qiao, A facile soft-template synthesis of mesoporous polymeric and carbonaceous nanospheres, *Nat. Commun.*, 2013, **4**, 2798–2801.

18 Y. T. Tan, D. S. Lin, C. Liu, W. C. Wang, L. Kang and F. Ran, Carbon nanofibers prepared by electrospinning accompanied with phase-separation method for supercapacitors: Effect of thermal treatment temperature, *J. Mater. Res.*, 2018, DOI: 10.1557/jmr.2017.373.

19 Z. Wang, Y. T. Tan, Y. Liu, L. Y. Niu, L. B. Kong, L. Kang and F. Ran, New amphiphilic block copolymer-modified electrodes for supercapacitors, *New J. Chem.*, 2018, **42**, 1290–1299.

20 Z. Wang, Y. T. Tan, Y. L. Yang, X. N. Zhao, Y. Liu, L. Y. Niu, B. Tichnell, L. B. Kong, L. Kang, Z. Liu and F. Ran, Pomelo peels-derived porous activated carbon microsheets dual-doped with nitrogen and phosphorus for high performance electrochemical capacitors, *J. Power Sources*, 2018, **378**, 499–510.

21 S. Dutta, A. Bhaumik and K. C. W. Wu, Hierarchically porous carbon derived from polymers and biomass: effect of interconnected pores on energy applications, *Energy Environ. Sci.*, 2014, **7**, 3574–3592.

22 Y. T. Tan, Y. Liu, L. B. Kong, L. Kang and F. Ran, Supercapacitor electrode of nano-Co3O4 decorated with gold nanoparticles via in-situ reduction method, *J. Power Sources*, 2017, **363**, 1–7.

23 J. Yan, T. Wei, B. Shao, Z. Fan, W. Qian, M. Zhang and F. Wei, Preparation of a graphene nanosheet/polyaniline composite with high specific capacitance, *Carbon*, 2010, **48**, 487–493.

24 Y. T. Tan, Y. S. Liu, Y. F. Zhang, C. A. Xu, L. B. Kong, L. Kang and F. Ran*, Dulse-derived porous carbon–polyaniline nanocomposite electrode for high-performance supercapacitors, *J. Appl. Polym. Sci.*, 2018, **135**(5), 45776.

25 Q. Wu, Y. Xu, Z. Yao, A. Liu and G. Shi, Supercapacitors based on flexible graphene/polyaniline nanofiber composite films, *ACS Nano*, 2010, **4**, 1963–1970.

26 Y. Liu, L. Y. Liu, Y. T. Tan, L. Y. Niu, L. B. Kong, L. Kang and F. Ran, Carbon nanosphere@vanadium nitride electrode materials derived from metal-organic nanospheres self-assembled by NH4VO3, chitosan, and amphiphilic block copolymer, *Electrochim. Acta*, 2018, **262**, 66–73.

27 A. M. Glushenkov, D. Hulicovajurcakova and D. Llewellyn, Structure and capacitive properties of porous nanocrystalline VN prepared by temperature-programmed ammonia reduction of V2O5, *Chem. Mater.*, 2010, **22**, 914–921.

28 P. J. Hanumantha, M. K. Datta and K. Kadakia, Vanadium nitride supercapacitors: effect of processing parameters on electrochemical charge storage behavior, *Electrochim. Acta*, 2016, **207**, 37–47.

29 Y. L. Yang, K. W. Shen, Y. Liu, Y. T. Tan, X. N. Zhao and F. Ran, Novel hybrid nanoparticles of vanadium nitride/porous carbon as an anode material for symmetrical supercapacitor, *Nano-Micro Lett.*, 2017, **9**, 6.

30 Y. G. Wu and F. Ran, Vanadium nitride quantum dot/nitrogen-doped microporous carbon nanofibers electrode for high-performance supercapacitors, *J. Power Sources*, 2017, **344**, 1–10.

31 D. K. Nandi, U. K. Sen and D. Choudhury, Atomic layer deposited molybdenum nitride thin film: a promising anode material for Li ion batteries, *ACS Appl. Mater. Interfaces*, 2014, **6**, 6606–6615.

32 D. Sun, J. Lang and X. Yan, Fabrication of TiN nanorods by electrospinning and their electrochemical properties, *J. Solid State Chem.*, 2011, **184**, 1333–1338.

33 B. A. Deore, I. Yu and M. S. Freund, A switchable self-doped polyaniline: interconversion between self-doped and non-self-doped forms, *J. Am. Chem. Soc.*, 2004, **126**, 52–53.

34 J. Liu, K. Huang and H. Tang, Porous and single-crystalline-like molybdenum nitride nanobelts as a non-noble electrocatalyst for alkaline fuel cells and electrode materials for supercapacitors, *Int. J. Hydrogen Energy*, 2016, **41**, 996–1001.

35 X. L. Li, Y. Xing, H. Wang, H. L. Wang, W. D. Wang and X. Y. Chen, Synthesis and characterization of uniform nanoparticles of γ-Mo2N for supercapacitors, *T. Nonferr. Metal Soc.*, 2009, **19**, 620–625.

36 X. Zhou, H. Chen and D. Shu, Study on the electrochemical behavior of vanadium nitride as a promising supercapacitor material, *J. Phys. Chem. Solids*, 2009, **70**, 495–500.

37 P. J. Hanumantha, M. K. Datta, K. S. Kadakia, D. Hong and S. Chung, A simple low temperature synthesis of nanostructured vanadium nitride for supercapacitor applications, *J. Electrochem. Soc.*, 2013, **160**, A2195–A2206.

38 Y. L. Yang, L. Zhao, K. W. Shen, Y. Liu, X. N. Zhao, J. Y. Wu and F. Ran, Ultra-small vanadium nitride quantum dots embedded in porous carbon as high performance electrode materials for capacitive energy storage, *J. Power Sources*, 2016, **333**, 61–71.

39 H. Wu, G. Chan, J. W. Choi, I. Ryu, Y. Yao, M. T. McDowell, S. W. Lee, A. Jackson, Y. Yang, L. Hu and Y. Cui, Stable cycling of double-walled silicon nanotube battery anodes

through solid-electrolyte interphase control, *Nat. Nanotechnol.*, 2012, **7**, 310–315.

40 B. Zhang, F. Kang, J. M. Tarascon and J. K. Kim, Recent advances in electrospun carbon nanofibers and their application in electrochemical energy storage, *Prog. Mater. Sci.*, 2016, **76**, 319–380.

41 X. Li, Y. Chen, H. Huang, Y. W. Mai and L. Zhou, Electrospun carbon-based nanostructured electrodes for advanced energy storage A review, *Energy Storage Mater.*, 2016, **5**, 58–92.

42 Y. Chen, X. Li, K. Park, J. Song, J. Hong, L. Zhou, Y. W. Mai, H. Huang and J. B. Good enough, Hollow carbon-nanotube/carbon-nanofiber hybrid anodes for Li-ion batteries, *J. Am. Chem. Soc.*, 2013, **135**, 16280–16283.

43 Y. Yu, L. Gu, C. Zhu, P. A. Van Aken and J. Maier, Tin nanoparticles encapsulated in porous multichannel carbon microtubes: preparation by single-nozzle electrospinning and application as anode material for high-performance Li-based batteries, *J. Am. Chem. Soc.*, 2009, **131**, 15984–15985.

44 L. Zhang, Y. Huang, Y. Zhang, H. Gu, W. Fan and T. Liu, Flexible electrospun carbon nanofiber@NiS core/sheath hybrid membranes as binder-free anodes for highly reversible lithium storage, *Adv. Mater. Interfaces*, 2016, **3**, 1500467.

45 M. Cao, L. Zhou, X. Xu, S. Cheng, J. L. Yao and L. J. Fan, Galvanic replacement approach for bifunctional polyacrylonitrile/Ag–M (M=Au or Pd) nanofibers as SERS-active substrates for monitoring catalytic reactions, *J. Mater. Chem. A*, 2013, **1**, 8942–8949.

46 X. Xiao, X. Peng, H. Jin, T. Li, C. Zhang, B. Gao, B. Hu, K. Huo and J. Zhou, Freestanding mesoporous VN/CNT hybrid electrodes for flexible all-solid-state supercapacitors, *Adv. Mater.*, 2013, **25**, 5091–5097.

47 L. Zhang, C. M. B. Hol, E. J. Luber, B. C. Olsen, H. Wang, M. Danaie, X. Cui, X. Tan, V. W. Lui, W. P. Kalisvaart and D. Mitlin, High rate electrochemical capacitors from three-dimensional arrays of vanadium nitride functionalized carbon nanotubes, *J. Phys. Chem. C*, 2011, **115**, 24381–24393.

48 C. M. Ghimbeu, E. Raymundo-Piñero, P. Fioux, F. Béguinb and C. Vix-Guterla, Vanadium nitride/carbon nanotube nanocomposites as electrodes for supercapacitors, *J. Mater. Chem.*, 2011, **21**, 13268–13275.

49 T. L. John, F. Debby and S. Ronald, Functional polymers from novel carboxylterminated trithiocarbonates as highly efficient RAFT agents, *Macromolecules*, 2002, **35**, 6754–6756.

50 H. L. Fan, F. Ran, X. X. Zhang, H. M. Song, W. X. Jing, K. W. Shen, L. B. Kong and L. Kang, Easy fabrication and high electrochemical capacitive performance of hierarchical porous carbon by a method combining liquid-liquid phase separation and pyrolysis process, *Electrochim. Acta*, 2014, **138**, 367–375.

51 X. N. Zhao, F. Ran, K. W. Shen, Y. L. Yang, J. Y. Wu, X. Q. Niu, L. B. Kong, L. Kang and S. W. Chen, Facile fabrication of ultrathin hybrid membrane for highly flexible

supercapacitors via in-situ phase separation of polyethersulfone, *J. Power Sources*, 2016, **329**, 104–114.

52 Z. P. Zhou and G. L. Liu, Controlling the pore Size of mesoporous carbon thin films through thermal and solvent annealing, *Small*, 2017, **13**, 1603107.

53 K. Xiao, L. X. Ding, H. Chen, S. Wang, X. Lu and H. Wang, Nitrogen-doped porous carbon derived from residuary shaddock peel: a promising and sustainable anode for high energy density asymmetric supercapacitors, *J. Mater. Chem. A*, 2016, **4**, 372–378.

54 K. Xiao, L. X. Ding, G. X. Liu, H. B. Chen, S. Q. Wang and H. Wang Freestanding, hydrophilic nitrogen-doped carbon foams for highly compressible all solid-state supercapacitors, *Adv. Mater.*, 2016, **28**, 5997–6002.

55 F. Cheng, C. He and D. Shu, Preparation of nanocrystalline VN by the melamine reduction of $V_2O_5$ xerogel and its supercapacitive behavior, *Mater. Chem. Phys.*, 2011, **131**, 268–273.

56 Y. U. M. Shulga, V. N. Troitskii and M. I. Aivazov, X-ray photo-electron spectra of the mononitrides of Sc, Ti, V and Cr Zh, *Neorg. Khim.*, 1976, **21**, 2621–2624.

57 B. Gao, X. Li and X. Guo, Nitrogen-doped carbon encapsulated mesoporous vanadium nitride nanowires as self-supported electrodes for flexible all-solid-state supercapacitors, *Adv. Mater. Interfaces*, 2015, **2**, 13.

58 X. Zhou, C. Shang and L. Gu, Mesoporous coaxial titanium nitride-vanadium nitride fibers of core–shell structures for high-performance supercapacitors, *ACS Appl. Mater. Interfaces*, 2011, **3**, 3058–3063.

59 V. Bondarenka, Valence of vanadium in hydrated compounds, *Lith. J. Phys.*, 2007, **47**, 333–342.

60 Y. Shul'Ga and V. N. Troitskii, Study of the surface of finely divided titanium nitride by X-ray photoelectron spectroscopy, *Rev. Mex. Biodivers.*, 2006, **18**, 681–684.

61 D. K. Nandi, U. K. Sen and D. Choudhury, Atomic layer deposited molybdenum nitride thin film: a promising anode material for Li ion batteries, *ACS Appl. Mater. Interfaces*, 2014, **6**, 6606–6615.

62 K. S. W. Sing, D. H. Everett, R. A. W. Haul, L. Moscou, R. A. Pierotti, J. Rouquero and T. Siemieniewska, Reporting physisorption data for gas/solid systems with special reference to the determination of surface area and porosity (Recommendations 1984), *Pure Appl. Chem.*, 1985, **57**, 603–619.

63 Z. Li, Z. Xu and X. Tan, Mesoporous nitrogen-rich carbons derived from protein for ultra-high capacity battery anodes and supercapacitors, *Energy Environ. Sci.*, 2013, **6**, 871–878.

64 A. Biedunkiewicz, U. Gabriel, P. Figiel and M. Sabara, Investigations on $NH_4VO_3$ thermal decomposition in dry air, *J. Therm. Anal. Calorim.*, 2012, **108**, 965–970.

65 J. Zhao, B. Liu, S. Xu, J. Yang and Y. Lu, Fabrication and electrochemical properties of porous VN hollow nanofibers, *J. Alloys Compd.*, 2015, **651**, 785–792.

66 R. Wang, X. Yan and J. Lang, A hybrid supercapacitor based on flower-like Co(OH)$_2$ and urchin-like VN electrode materials, *J. Mater. Chem. A*, 2014, **2**, 12724–12732.

67 H. Yan, X. Dong and Z. Cui, Hierarchical porous carbon hollow-spheres as a high performance electrical double-layer capacitor material, *J. Power Sources*, 2012, **211**, 92–96.

68 Y. Xu, J. Wang, L. Shen, H. Dou and X. Zhang, One-dimensional vanadium nitride nanofibers fabricated by electrospinning for supercapacitors, *Electrochim. Acta*, 2015, **173**, 680–686.

This journal is © The Royal Society of Chemistry 2018